Spin waves and temperature-dependent behaviour of the quasi-two-dimensional antiferromagnet $KFeF_4$

1994 J. Phys.: Condens. Matter 6 6667

(http://iopscience.iop.org/0953-8984/6/33/014)

J. Phys.: Condens. Matter 6 (1994) 6667–6678. Printed in the UK

Spin waves and temperature-dependent behaviour of the quasi-two-dimensional antiferromagnet $KFeF_4$

S Fulton†, S E Nagler‡, L M N Needham§ and B M Wanklyn†

† Oxford Physics, Clarendon Laboratory, Oxford, UK

‡ Department of Physics, University of Florida, Gainesville, FL, USA

§ Department of Physics, Warwick University, Coventry, UK

Received 12 April 1994, in final form 20 May 1994

Abstract. A study of the quasi-two-dimensional antiferromagnet $KFeF_4$ below the transition temperature, T_N = 13 K, has been undertaken using neutron scattering techniques. The dispersion relation of the spin excitations is well described by a model Hamiltonian incorporating Heisenberg exchange interactions and uniaxial anisotropy. The anisotropy controls the energy of the zone centre mode whose frequency varies in the same way with temperature as the square of the staggered magnetization which is described by the two-dimensional Ising model. Dipole–dipole contributions are too small to account fully for the anisotropy. Different nearest-neighbour exchange energies are found along the a and b directions due to different superexchange paths, with $J_1 = -2.18$ meV along a, and $J_2 = -2.73$ meV along b.

1. Introduction

The magnetic behaviour of a system depends on the dimensionality and the nature of the magnetic interactions. Layered antiferromagnets with the K_2MnF_4 structure are excellent examples of two-dimensional systems with relatively simple magnetic interactions. Linear spin-wave theory has proved to be a very successful model for the spin-wave energies, incorporating a Heisenberg exchange interaction between nearest neighbours within the planes and a small Ising anisotropy to simulate the effect of dipolar interactions or crystal field effects [1]. The critical properties close to the phase transition are dominated by the Ising behaviour and two-dimensional Ising model exponents are obtained [2]. At higher temperatures this is not the case and the systems are found to have a crossover from the Ising model to behaviour dominated by the two-dimensional Heisenberg interactions [3].

The two-dimensional Heisenberg model has recently attracted considerable theoretical attention because it is found to be an appropriate model for the undoped cuprate systems. Chakravarty *et al* [4] have developed a theory for the two-dimensional quantum Heisenberg antiferromagnet (QHAF) based on a renormalization of the classical model developed by Shenker and Tobochnik [5]. This QHAF successfully describes the experimental results from both La_2CuO_4 (S = 1/2) [4] and K_2NiF_4 (S = 1) [3].

The purpose of this study is to characterize the magnetic properties of the analogous system $KFeF_4$, which has S = 5/2 and so approximates more closely the classical spin model. In the next section we describe the structure of $KFeF_4$ and discuss the linear spin-wave model used to describe the interactions. Section 3 details the experimental arrangement and in section 4 the neutron scattering measurements of the spin waves are

0953-8984/94/336667+12$19.50

outlined, and the strength of the magnetic interactions deduced. These interactions are used to calculate the form of the two-magnon Raman scattering and this is compared to experimental measurements in section 5.

After the magnetic interactions had been characterized a study of the critical behaviour was undertaken. Section 6 describes measurements of the temperature dependence of the sub-lattice magnetization and of the spin-wave gap frequency. The results show that both have behaviour which is characteristic of the two-dimensional Ising model. In a forthcoming paper (paper II, [27]) we describe the nature of the critical fluctuations above T_N, and compare the results with those predicted by the various two-dimensional models.

A brief preliminary account of these neutron scattering results has already been presented [6]. The results for the spin-wave spectrum are consistent with those of Desert *et al* [7], in so far as they overlap, but the results in this paper extend the knowledge of the magnetic interactions.

2. Structure and magnetism

$KFeF_4$ has a layered structure in which the Fe^{3+} ions lie in the *ab*-planes and each Fe^{3+} is surrounded by six F^- ions forming an octahedron [8]. Unlike the tetragonal K_2MnF_4 structures $KFeF_4$ is orthorhombic, due to the tilting of the fluorine octahedra out of the plane along the a direction at angle of 11.64° to the horizontal [8]; see figure 1. This leads to a doubling of the unit cell along the a-axis. Below 360 K there is a further distortion of the system caused by a rotation of the octahedra about the c-axis by 8° with the consequence of doubling the unit cell along the b-axis and leading to a space group of *Pcmn* and lattice constants at 50 K of $a = 7.564$ Å, $b = 7.750$ Å, $c = 12.27$ Å. The details of the structure have been determined by x-ray scattering [9] and are consistent with Raman scattering measurements [10]. The crystal and magnetic lattices are identical in this system due to the distortion in the crystal structure.

The Fe^{3+} ion has a half-filled 3d shell with $S = 5/2$ and has no orbital angular momentum in its ground state, $L = 0$. Symmetry arguments in $KFeF_4$ lead to the magnetic interactions between nearest-neighbour layers cancelling out [11], just as in the K_2MnF_4 structures. This means the interlayer magnetic interactions are much weaker than the intralayer interactions, the ratio being of the order of 10^{-4}, and thus $KFeF_4$ can essentially be treated as a two-dimensional antiferromagnet. When modelling the spin-wave dispersion relation, the distortion due to the rotation of the octahedra allows the two nearest-neighbour exchange energies, one along the a and the other along the b direction to be different. An Ising anisotropy term has also been included in the Hamiltonian, and this aligns the spins in their preferred direction along the crystallographic c-axis. Using linear spin-wave theory as discussed by Keffer [12] the dispersion relation for a two-dimensional antiferromagnet with nearest-neighbour and next-nearest neighbour interactions was obtained as

$$E_q^2 = \left[g\mu_B H_A - 2S(J_1 + J_2) + 4SJ_3 - 2SJ_3\left(\cos\tfrac{1}{2}(q_x a + q_y b) + \cos\tfrac{1}{2}(q_x a - q_y b)\right)\right]^2 - \left[2S\left(J_1 \cos\tfrac{1}{2}(q_x a) + J_2 \cos\tfrac{1}{2}(q_y b)\right)\right]^2. \quad (1)$$

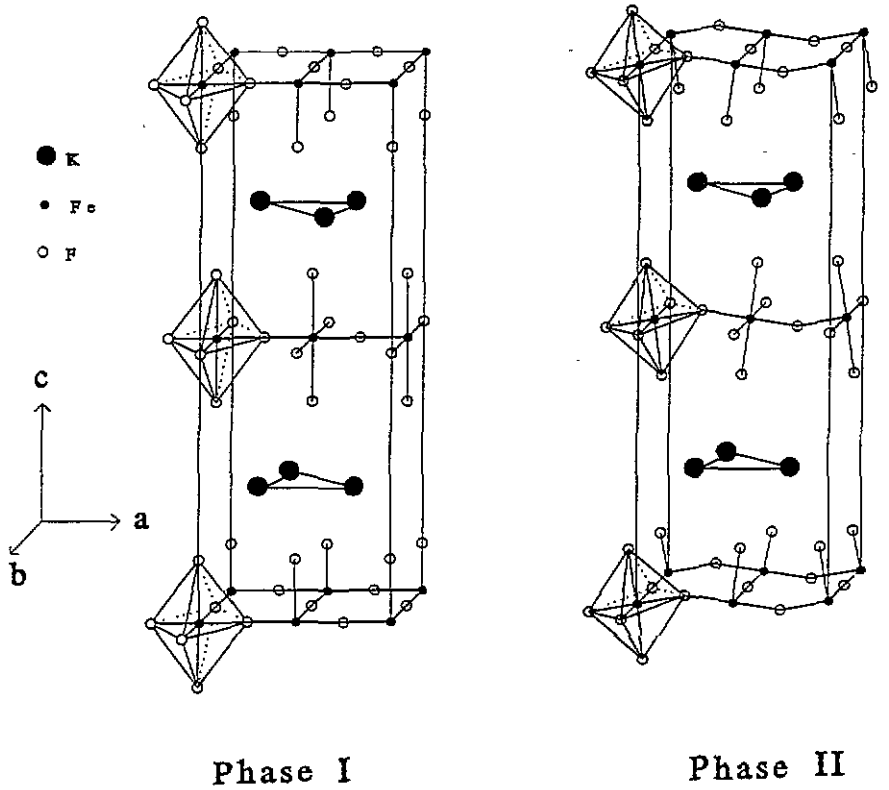

Figure 1. Phase I—the ideal crystal structure of $KFeF_4$. Phase II—the fluorine octahedra have rotated about the b-axis by 11.6° doubling the a lattice parameter.

Equation (1) represents the energies of the spin waves with wave vector q, J_1 and J_2 are the nearest-neighbour exchange interactions in the a and b directions respectively, and J_3 is the next-nearest-neighbour interaction. The exchange energies have been written as $-J\sum \boldsymbol{S}_i \cdot \boldsymbol{S}_j$, and the effective field due to the anisotropy effects is represented by H_A.

3. The experimental set-up

The $KFeF_4$ crystal was grown at the Clarendon Laboratory using the flux growth method [13]. The crystal was a small plate 11 mm × 7 mm × 2 mm and was found to contain two crystallites 2° apart. The mosaic spread in the ab-plane was found to be 0.5°.

The neutron scattering experiments were performed at the ILL in Grenoble using the thermal guide triple-axis crystal spectrometer IN3, with a copper monochromator and a pyrolytic graphite analyser. The scattered neutron energy was held fixed at 14.7 meV and a pyrolytic graphite filter on the scattered side was used to reduce the scattering of higher energy neutrons by the (004)-planes of the analyser. The collimation of the instrument when measuring the dispersion relation was 20′ before the monochromator, 40′ between

the monochromator and sample, 40′ between the sample and analyser and 40′ between the analyser and detector. This was changed to 20′–20′–20′–30′ before the data for the temperature dependence of the staggered magnetization and the anisotropy gap was taken. The crystal was aligned with the c axis perpendicular to the beam so that spin waves propagating in the ab-plane could be examined. The crystal was placed in a variable-temperature cryostat which controlled the temperature to an accuracy of ±0.01 K.

4. The spin-wave dispersion relation

The spin-wave dispersion curves were determined by controlling the spectrometer so that the wavevector transfer, $\boldsymbol{Q}$, was held constant while the energy was scanned. This yielded well defined spin-waves as shown in figures 2 and 4. The scans were taken round about the (220) and (310) magnetic reciprocal lattice points where the magnetic lattice is the same as the crystal lattice. The spin waves were determined for three propagation directions [$\xi\xi$0], [ξ00] and [0ξ0] at 50 K so that the difference in exchange interactions in the a and b directions could be investigated. ξ is the reduced wave vector, which for the a direction is given by $q_x a/2\pi$, and similarly for the b direction. Data were also collected at 100 K for the [$\xi\xi$0] direction.

The spin-wave energies were determined by fitting the scans to Gaussians using the Marquadt least-squares fit method [14] and examples of fits to the data are shown in figure 2. The resulting dispersion curves are shown in figure 3 and the solid line represents the best fit to the experimental data given by equation (1).

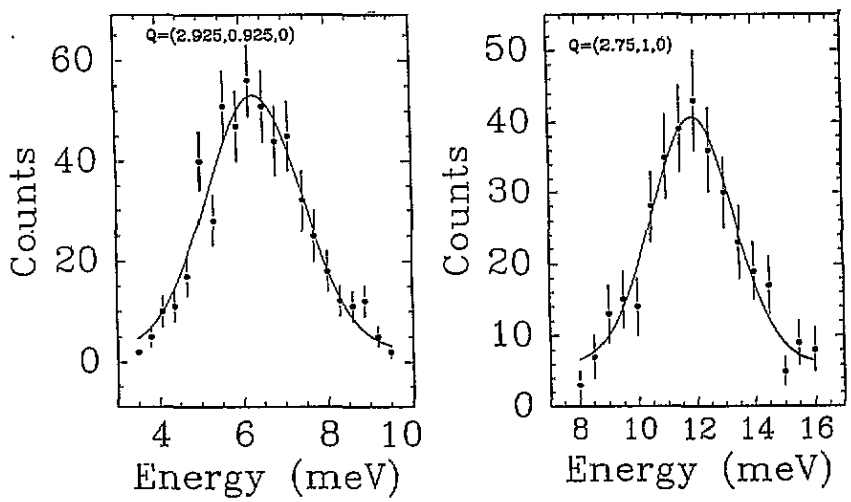

Figure 2. Neutron scattering observed with constant-Q scans and fits to Gaussians to find the peak position.

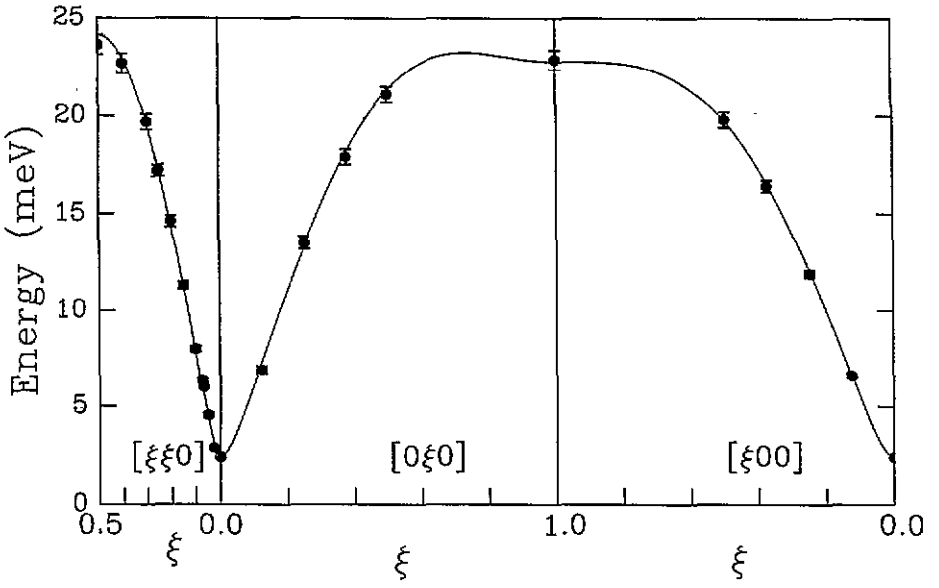

Figure 3. The spin-wave dispersion curves of $KFeF_4$ at 50 K. The solid line represents a fit to equation (1).

Table 1. The model parameters found from the spin-wave dispersion curves.

	J_1 (meV)	J_2 (meV)	J_3 (meV)	$g\mu_B H_A$ (meV)	Normalized χ^2
50 K	−2.10±0.02	−2.68±0.04	–	0.123±0.003	1.94
50 K	−2.26±0.08	−2.78±0.06	0.12±0.04	0.116±0.004	1.72
100 K ($J_1 = J_2$)	−2.40±0.06	−2.40±0.06	—	0.1 (fixed)	6.99

Two fits were made to the measured curves at 50 K; one including the nearest-neighbour interactions only and the other allowing for nearest and next-nearest-neighbour interactions. Fits to the 100 K data only allowed for nearest-neighbour interactions. The values for the exchange constants obtained from these fits are listed in table 1. An average from the two 50 K fits gives $J_1 = -2.18$ meV, $J_2 = -2.7$ meV with the next-nearest-neighbour interaction being about twenty times smaller in magnitude. These results are in good agreement with the previous studies listed in table 2. A nearest-neighbour exchange constant of −2.30 meV was obtained from susceptibility measurements [15], −2.35 meV from Raman scattering measurements [18] and −2.44 meV from neutron scattering measurements [7] all of which measured the average of J_1 and J_2. Our results show a surprisingly large difference in nearest-neighbour exchange constants J_1 and J_2. The difference arises from the different superexchange paths in the a and b directions due to the tilting of the fluorine ions out of the plane in the a direction [8], thus making J_1 smaller than J_2, even though the lattice constant a is smaller than b. This result can be qualitatively explained by the superexchange theory of Anderson [16].

When the superexchange occurs through F^- ligand p electrons, the strongest coupling occurs when the magnetic ions are diametrically opposite. Using simple geometric

Table 2. The parameters found from previous studies on $KFeF_4$.

	$J_1 = J_2$ (meV)	$g\mu_B H_A$ (meV)
Neutron scattering [7]	−2.44	0.11
Raman scattering [18]	−2.35	0.10
Susceptibility [15]	−2.30	0.11

arguments, and considering only the change in the overlap of the wavefunctions as the bond angle between the magnetic ions changes, suggests relations between the undistorted exchange path in the *b* direction, J_2, and J_1 in the distorted *a* direction of the form

$$J_1 = J_2 \cos^4 \theta \tag{2}$$

or

$$J_1 = J_2 \cos^2(2\theta) \tag{3}$$

where $\theta = 11.64°$ and is the angle of tilt from the horizontal. These suggest that if J_2 is equal to −2.73 meV, J_1 would be −2.51 meV (equation (2)) or −2.30 meV (equation (3)) whereas the measured value is −2.18 meV. These simple geometric arguments do not fully account for the difference in the exchange energies, but do explain why there is a reduction of an appropriate order of magnitude.

The value obtained for the anisotropy energy, $g\mu_B H_A = 0.12$ meV, is approximately four times larger than expected from the dipolar interactions (0.033 meV) [17], and thus there must be other contributions which should be taken into account when calculating H_A, which are not important in the analogous Rb_2MnF_4 with $S = 5/2$ ions [15]. At present we do not have a convincing explanation for this difference. It has been suggested by Abdalian *et al* [18] and by Desert [7] that the additional anisotropy may be related to residual Fe^{2+} ions present in the crystal, but all the studies using different samples have found similar values for the extra anisotropy and in K_2FeF_4 [19] the preferred orientation for the Fe^{2+} ($S = 2$, $L = 2$) spins within a fluorine octahedral environment is along the [110] axis, that is in the plane. Fe^{2+} would then tend to lower the average anisotropy trying to align the spins along the *c* axis not increase it.

Another possibility is that the distorted tetragonal structure of $KFeF_4$ gives rise to anisotropic exchange interactions of the Dyzaloshinski form as found in $LaCuO_4$ [20]. Such interactions would give rise to a splitting of the degenerate spin-wave modes and so we performed careful high-resolution measurements. The results are shown in figure 4 together with a computer simulation of the expected profile calculated using the program RESCAL which numerically convolves the resolution of the instrument (calculated from the formalism of Cooper and Nathans [21]) with the spin-wave dispersion. Clearly there is no evidence for any splitting. This is in agreement with a similar study of Desert [7]. A further possibility is that the cubic crystal field on the Fe^{3+} ions is sufficiently large that the weak

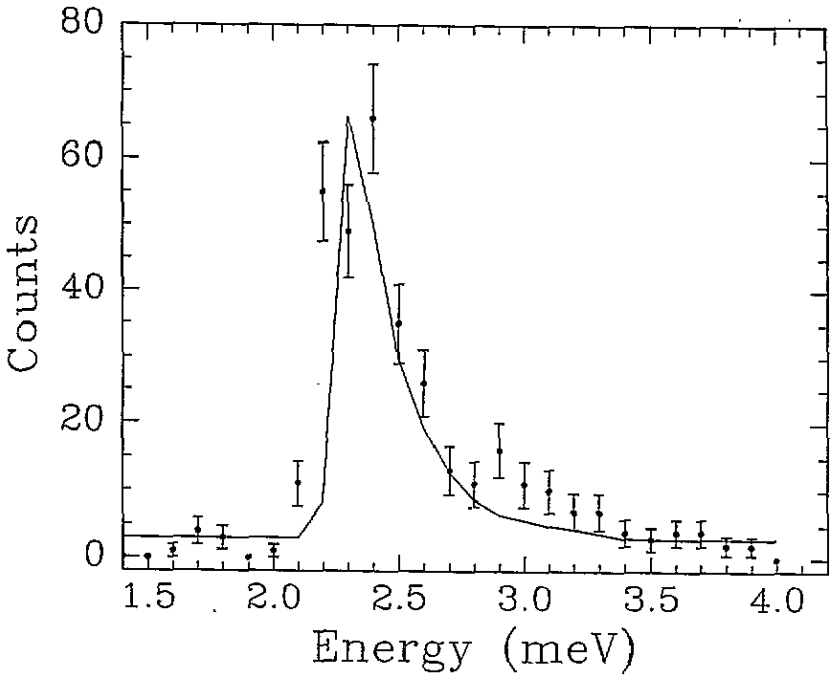

Figure 4. The scattering observed at the zone centre. The solid line is a simulation of the data using the resolution function convolved with the dispersion relation.

crystal field result ($L = 0$, $S = 5/2$) is inadequate. Abragam and Bleaney [22] show that a strong crystal field produces a lowering of the energy of the $^2\Gamma_5$ component of the $S = \frac{1}{2}$, $L = 6$ atomic state. The non-cubic terms in the crystal field and the spin–orbit interaction might then mix this state with the $^6\Gamma_1$ weak crystal field ground state leading to some anisotropy in the ground state wavefunction and hence to anisotropy in the interactions. Unfortunately, the strength of the crystal fields is unknown and it is not possible to make a quantitative calculation.

5. Comparison with the two-magnon Raman scattering

In the two-magnon Raman scattering study carried out by Abdalian *et al* [18] at 2 K, it was noted that the exchange constant extracted from the Raman profile was 4% smaller than the exchange constant obtained from the same sample using neutron scattering techniques [7] at 15 K. In that neutron scattering study the dispersion curves were measured in only one direction [110], and thus the different exchange interactions in the a and b directions were not seen. We have repeated the simulation of the Raman profile [23, 24] using the exchange constants obtained from our neutron scattering experiment, which gave different exchange constants along the a and b directions, in order to see if our more realistic spin-wave model accounted for the discrepancy. A comparison of the simulation with the experimental data is shown in figure 5. This calculation is based on the theory developed by Elliot and

Thorpe [23] and takes into account the spin-wave interactions which lower the expected peak frequency from that obtained by the classical non-interacting approach. It is seen that taking into account the different nearest-neighbour exchange constant does not account for the 4% discrepancy in the value of the exchange constant extracted from the Raman data, and thus it is not clear why this difference arises.

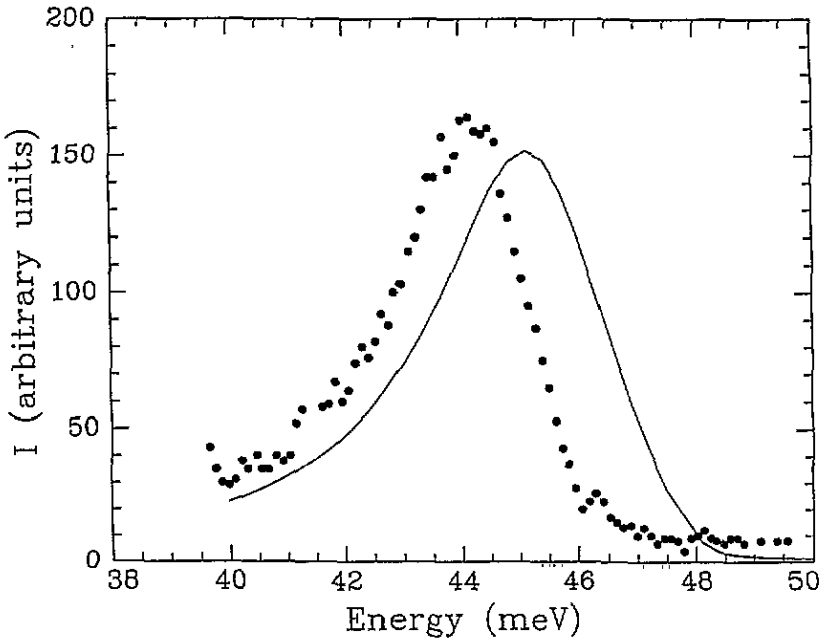

Figure 5. Comparison of the Raman scattering [18] (dots) with a calculation based on interacting magnon theory [22, 23] (line).

Table 3. Results of the fits to power law behaviour below T_N.

	c	T_N (K)	Normalized χ^2
Anisotropy gap	0.26±0.01	137.0±0.5	2.8
(1, 1, 0) integrated intensity	0.26±0.01	137.0±0.3	2.3

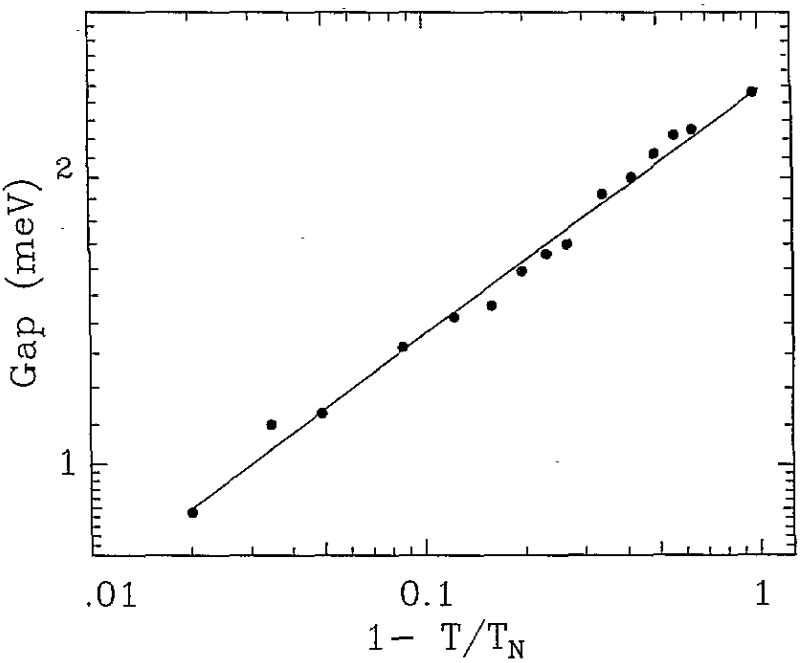

Figure 6. Variation of the spin-wave gap energy with reduced temperature. The line is a fit to power law behaviour.

6. Temperature dependence below T_N

The temperature dependence of the effective anisotropy in the dispersion relation at the magnetic zone centre was measured as described in section 3. The data were collected with the wavevector transfer Q fixed at the zone centre $(1, 1, 0)$ and scanning the energy transfer while keeping the final neutron energy fixed at 14.7 meV. The peak energy of the spin waves at the zone centre were extracted from the data by fitting to Gaussians. The results are shown in figure 6 along with power law fits to the data. The parameters extracted from these fits are shown in table 3 where

$$\omega = B\left[\frac{T_N - T}{T_N}\right]^c. \tag{4}$$

Measurements of the integrated Bragg intensity of the magnetic reflections were also made at various temperatures below T_N, so that the temperature dependence of the magnetic order parameter could be obtained. The Bragg reflections were scanned in Q along [110] as shown in figure 7 and the total intensity of the peak was used to give a measure of the integrated intensity at each temperature. The integrated intensity of the magnetic Bragg peaks is proportional to the square of the staggered magnetization, which is predicted to have power law behaviour with a critical exponent 2β. The results of the integrated

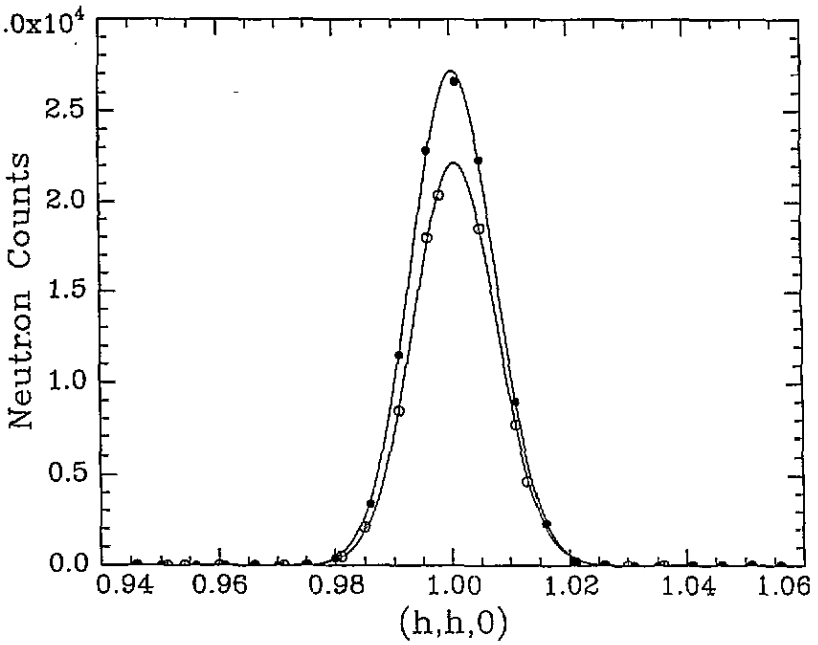

Figure 7. The scattered intensity from the (110) magnetic Bragg peak at T = 60 K (filled circles) and T = 105 K (open circles). The solid lines are fit to obtain the integrated intensity.

intensity measurements are shown in figure 8 along with a fit to the power law behaviour (equation (4)).

Comparing the results from the two fits (table 3), it is seen that the anisotropy gap varies in the same way as the integrated intensity of the (110) magnetic Bragg reflection, so that $c = 2\beta$, and the critical exponent β describing the temperature dependence of the order parameter is 0.130±0.005, in agreement with 0.125 for a two-dimensional Ising system [25]. Thus the anisotropy energy varies in the same way as the square of staggered magnetization as was also found in the analogous layered system K_2NiF_4 [26].

7. Conclusions

The spin-wave excitations of $KFeF_4$ are well described by a two-dimensional spin Hamiltonian incorporating nearest-neighbour and next-nearest-neighbour Heisenberg exchange interactions and an anisotropy term. The different superexchange paths in the a and b directions lead to J_1 in the a direction being smaller than J_2 in the b direction. In agreement with other studies on $KFeF_4$, it is found that the dipole–dipole interactions do not account for the size of the anisotropy energy and it is suggested that a strong crystal field mixing may be responsible for the energy. This model does not explain the frequency of the peak in the Raman scattering data. The spin-wave gap is found to vary with temperature in the same way as the square of the staggered magnetization and the exponent is consistent

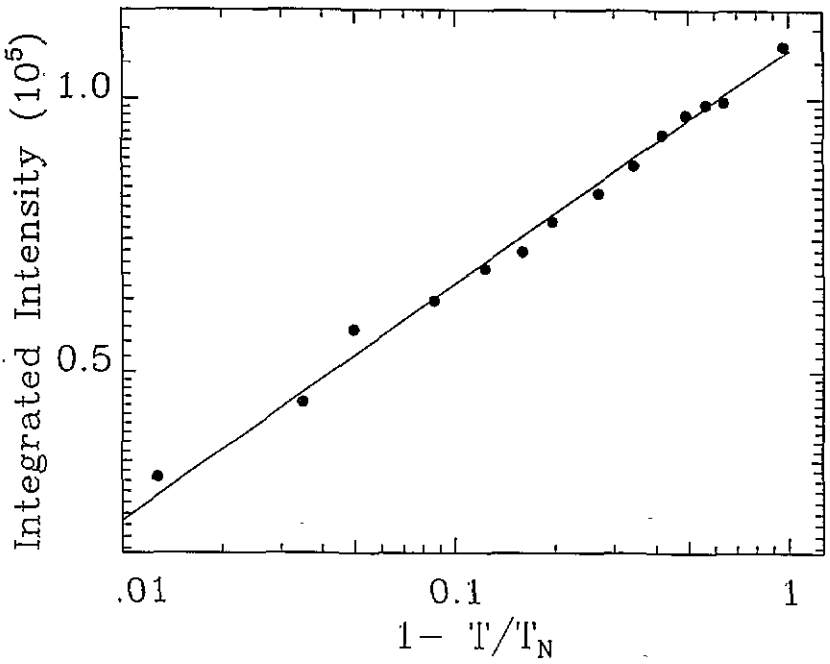

Figure 8. Variation of the integrated intensity of the (110) magnetic Bragg peak with reduced temperature. The line is a fit to power law behaviour.

with two-dimensional behaviour. Below T_N, β is found to be in good agreement with the two-dimensional Ising model value.

Acknowledgments

We are grateful for a helpful suggestion by the referee. Financial support was provided by the SERC for experiments at the Institut Laue–Langevin and work in Oxford.

References

[1] Birgeneau R J, Guggenheim H J and Shirane G 1973 *Phys. Rev.* B **8** 304
[2] Birgeneau R J, Als-Nielsen J and Shirane G 1977 *Phys. Rev.* B **16** 280
[3] Birgeneau R J 1990 *Phys. Rev.* B **41** 2514
[4] Chakravarty S, Halperin B and Nelson D R 1989 *Phys. Rev.* B **39** 2344
[5] Shenker S H and Tobochnik J 1980 *Phys. Rev.* B **9** 4469
[6] Fulton S, Nagler S E, Cowley R A and Needham L M 1992 *Physica* B **180 & 181** 25
[7] Desert A, Bulou A and Nouet J 1992 *Solid State Commun.* **83** 505
[8] Heger G and Geller R 1971 *Solid State Commun.* **9** 35
[9] Sciau P and Grebille D 1989 *Phys. Rev.* B **39** 11 982
[10] Desert A, Bulou A and Nouet J 1992 *J. Phys.: Condens. Matter* **4** 1023

[11] De Jongh L J and Meidema A R 1974 *Adv. Phys.* **23** 1
[12] Keffer F 1966 *Handbuch der Physik* vol 18II, (Berling: Springer) p 103
[13] Wanklyn B M 1975 *J. Mater. Sci.* **10** 1487
[14] Press W H, Flannery B P, Teukobly S A and Vellig W T 1988 *Numerical Recipes* (Cambridge: Cambridge University Press) ch 14
[15] Eibschutz M, Davidson G R and Guggenheim H J 1972 *AIP Conf. Proc.* 5 670
[16] Anderson P W 1950 *Phys. Rev.* 7 350
[17] De Wijn H W, Walker L R and Walsted R E 1973 *Phys. Rev.* B **8** 285
[18] Abdalian A T, Desert A, Dugaulier C, Bulou A, Moch P and Nouet J 1992 *J. Magn. Magn. Mater.* **104–107** 1047
[19] Thurlings M P, Frikkee E and De Wijn H W 1980 *J. Magn. Magn. Mater.* **15–18** 369
[20] Peters C J, Birgeneau R J, Kastner M A, Yoshizawa H, Endoh Y, Tranquanda J, Shirane G, Hidaka Y, Oda M, Suzuki M and Murakami T 1988 *Phys. Rev.* B **37** 9761
[21] Cooper M J and Nathans R 1967 *Acta Crystallogr.* **23** 357
[22] Abragam A and Bleaney B 1970 *Electron Paramagnetic Resonance of Transition Ions* (Oxford: Clarendon) p 482
[23] Elliott R J and Thorpe M F 1960 *J. Phys. C: Solid State Phys.* 2 1630
[24] Parkinson J B 1960 *J. Phys. C: Solid State Phys.* 2 2012
[25] Collins M F 1989 *Magnetic Critical Scattering* (Oxford: Oxford University Press)
[26] Birgeneau R J, De Rosa F and Guggenheim H J 1970 *Solid State Commun.* **8** 13
[27] Fulton S, Cowley R A, Desert A and Mason T 1994 *J. Phys.: Condens. Matter* **6** 6679–90